Effect of early stages of thermomechanical processing on inclusions in high carbon steel

FARAJI, Masoumeh, WILCOX, DP, THACKRAY, RP, TODD, I, HOWE, AA and TSAKIROPOULOS, A

Published version

FARAJI, Masoumeh, WILCOX, DP, THACKRAY, RP, TODD, I, HOWE, AA and TSAKIROPOULOS, A (2014). Effect of early stages of thermomechanical processing on inclusions in high carbon steel. Materials Science and Technology, 30 (10), 1177-1188.

Effect of early stages of thermomechanical processing on inclusions in high carbon steel

M Faraji[1], DP Wilcox[2], R Thackray[1], I Todd[1], AA Howe[1] and P Tsakiropoulos[1]
1: The University of Sheffield
2: Tata Steel UK,

Key words: Inclusions, Cast Alloy, Plain Carbon Steel, Characterisation, thermomechanical processing

ABSTRACT

The effect of heat treatment and thermomechanical processing on size, size distribution, distribution and chemistry of non-metallic inclusions in a continuously cast high carbon steel was investigated using a Gleeble hot compression simulator at temperatures of 1050 and 1150°C and strains of 0.3 and 0.7 at strain rate 1/sec. The results showed that the total number of inclusions classified into three main types, namely sulphide, oxide and duplex, was reduced after the deformation at high temperature. Inclusions of different size and chemistry were found being present in different locations of the bloom and which was related with micro-segregation in the as-cast bloom. This suggested that inclusions were influenced by solidification conditions and sub-solidus homogenisation. Furthermore, the observed changes of chemistry of inclusions during heat treatment and thermomechanical processing at high temperature (~1100°C) are discussed. These changes were substantiated by evidence of devitrification of oxide inclusions including different manganese silicates.

INTRODUCTION

Non-metallic inclusions, in particular oxides, even when present at small volume fractions, can affect the mechanical properties of steels. There are two major groups of non-metallic inclusions in steel, namely sulphides and oxides[1] and the latter can include duplex type inclusions, for example oxide/sulphide ones[2] in which different oxides are surrounded by sulphide. Inclusions are also classified as indigenous and exogenous according to their mechanism of formation. Indigenous types, which themselves are classified as primary and secondary, are formed either as a result of reactions in the liquid melt and precipitation before solidification or precipitation from the steel during cooling and solidification. In contrast, exogenous inclusions, which are mainly oxides, are those formed as a result of erosion or corrosion of different materials such as refractories and slags; these, are sometimes defined as "mechanically entrained" inclusions[1]. Irrespective of their origins, it is believed that oxide inclusions are deleterious to the mechanical properties of steels as they are brittle and can act as stress risers in the matrix[3].

This work is focused on the effect of deformation at high temperature on the chemistry, morphology, size, size distribution and distribution of oxide and duplex inclusions and compares different sets of data obtained from the as-cast and deformed specimens. It also looks at the effect of heat treatment on different characteristics of inclusions and compares this data with the as-cast and deformed conditions.

EXPERIMENTAL

A continuously cast (283 x 230 mm, casting speed 1.3 m/min) high-carbon, manganese-silicon killed steel (Fe-0.77C-0.24Si-0.63Mn (wt%)) was supplied by Tata Steel UK. Cylindrical specimens (12 mm in diameter and 15 mm in length) were taken from different parts of the cast steel (Figure 1) so that comparisons can be made between inclusions in specimens taken from sub-surface areas (AAE

and AAM) with specimens taken from different depths into the bloom (DE, DM and EE, EM respectively 30-35 mm and 140 mm below the surface).

The cast specimens were prepared according to standard metallographic procedures for light microscopy and SEM-EDS study. Following characterisation of the inclusions in the cast steel using an automated FEI Quanta FEG-SEM equipped with EDAX Genesis EDS (Ref. 2) the same specimens were subjected to compressive deformation using a Gleeble 3800 Thermomechanical Simulator at two different temperatures of 1050 and 1150°C with strains of 0.3 and 0.7. The deformation parameters were as follows: heating for 2 minutes, holding for 30 seconds, deforming at strain rate of 1 /s and finally cooling with a rate of 20°C/sec. It should be noted that one specimen taken from sub-surface was only exposed to 1150°C (Table 1). After hot deformation, the inclusions in the deformed specimens were analysed using the same automated SEM technique and manually using a JEOL 6400 SEM equipped with INCA EDS. Table 1 summarises the studied materials, conditions and the studied areas. In the automated analyses the data was collected with X2700 magnification and covered 475 adjacent fields of 100 x 78.3 μm^2 over a 2 x 2 mm^2 area. In the manual data collection, the magnification and studied area varied depending on the size of inclusions and were respectively X1000 to X5000 and 2.3 to 14.5 mm^2.

Three main types of inclusions were observed in the cast steel, namely sulphides, oxides and duplex inclusions (mainly cores of Al_2O_3, or SiO_2 surrounded by MnS) (Ref. 2). To classify the oxide inclusion types, two different methods were used based on the data collection techniques. In automated microscopy oxides and sulphide inclusions were distinguished according to their grey level threshold; for the duplex inclusions further manual work was required to differentiate them according to their recorded coordinates in the specimen (e.g. if for two different types of inclusions, sulphide and oxide, the same coordinate was recorded, then those inclusions corresponding to that coordinate would be classified as one duplex inclusion); in manual microscopic characterisation the inclusions were classified according to their chemical compositions determined by EDS.

RESULTS and DISCUSSION

Characterisation of oxide type inclusions

The inclusions present in the cast steel were MnS, oxides (the majority of oxides contained more than one oxide component) and duplex oxide/sulphide inclusions[2]. In this work, the study of the inclusions in the deformed steel focused on oxides and duplex inclusions. The oxide inclusion types were divided into thirteen sub-groups, namely Aluminate, High Silica, Mg Silicates, Mn Silicate, Spessartite ($3MnO.Al_2O_3.3SiO_2$), Pseudo-Wollastonite ($CaSiO_3$), High Alumina, Anorthite ($CaO\cdot Al_2O_3\cdot 2SiO_2$), Gehlenite ($2CaO\cdot Al_2O_3\cdot SiO_2$), 20% Alumina Valley, Anorthite/Gehlenite Valley, Ca Silicates and Other (see (Ref. 2)). Figure 2 shows inclusions in deformed specimens taken from different areas of the bloom. Figure 3 shows evidence for phase transformations in inclusions, which could include crystallisation of glassy inclusions. Using the above classification, Figure 4 shows the percentages of different oxide inclusion types in different areas of the cast and deformed steel and Figure 5 includes this data for the heat treated specimen.

Figure 4 shows that the percentage of Mn silicate was reduced after hot deformation. In specimens taken from the sub-surface area this reduction was compensated by an increase in high silica and others; whereas in specimens taken from 30 mm below the surface and the bulk there was increase in the percentages of pseudo- wollastonite and 20% alumina valley. These changes were accompanied by changes in the content of Mn silicate constituents in specimens taken from different areas of the bloom that led to changes of the MnO to SiO_2 ratio in Mn silicates and to changes of the Al_2O_3 and CaO content, which are presented in figures 6 to 7.

Figures 6 to 7 show ternary SiO_2, Al_2O_3, RO (RO = the remaining components mainly MgO-CaO-MnO-TiO_2-K_2O) diagrams for different areas of the bloom, where the coordinates represent different oxide types (either from pure oxide or from oxide core of the duplex inclusions) observed within the studied areas for the as-cast and deformed bloom and for the heat treated specimen[2]. Figure 6 shows ternary diagrams for the sub-surface, 30 mm into the bulk and central area of the bloom, where the coordinates represent different oxide types observed within the studied area for the cast and deformed conditions and Figure 4 shows percentages of different oxide types for these specimens in bar-chart form. These two Figures show that in specimens taken from the sub-surface area, the oxide particles become more SiO_2 rich after deformation. Comparison of ternary diagrams for the sub-surface, 30 mm below the surface (quarter bulk) and the bulk area of the bloom in Figure 6 shows an opposite trend in chemical composition after hot deformation for quarter bulk and bulk compared with sub-surface area: Unlike the sub-surface regions, after hot deformation oxide inclusions become leaner in SiO_2. Figure 4 also gives the proportion of different oxide types for specimens taken from sub-surface, 30 mm below the surface and the bulk of the bloom. Figure 7 shows the ternary diagram comparing three different conditions, namely as-cast, heat-treated and deformed, for a specimen from the sub-surface area (AAE). The figure 7 shows a trend of oxides changing towards higher SiO_2 after heat-treatment and hot deformation.

It is worth mentioning that it was shown that there is a microsegregation of Si and Mn in the as-cast bloom where the maximum occurred in the DE and DM areas (Figure 8)[4]. The data would thus suggest that oxide inclusion formation in the continuously cast steel of this study was controlled by differences in the concentrations of Si and Mn in the melt between the surface areas and the bulk of the solidifying bloom; although this wasn't significant. Therefore, it is fair to say that the not-significant differences in general microsegregation level, if not controlling, could at most have a contributory effect to the oxide inclusion formation.

Looking at detailed oxide analysis of different specimens (refer to Table 4 in Ref. 2) revealed that compared with the cast steel, in the deformed steel there are content variations within oxide species depending on their location. This variation has been summarized in Table 2a. Table 2b also shows the oxide content variations for different oxide categories for specimen taken from sub-surface as a result of heat treatment.

The data presented in Tables 2a and 2b would thus suggest that the exposure to high temperature (and/or deformation) affected mainly (a) Mn silicates and anorthite via changes in MnO and Al_2O_3 contents, (b) pseudo-wollastonite and spessartite via changes in MnO, Al_2O_3 and TiO_2 content, (c) 20% alumina valley via changes in MnO, TiO_2 and CaO content, (d) anorthite via changes in CaO and (e) spessartite via changes in SiO_2 and Al_2O_3, (f) high silica via changes in MnO and/or Al_2O_3, TiO_2 where, an increase in Al_2O_3 and decrease in MnO content was observed for subsurface area whereas, the trend for MnO was opposite in 30 mm depth.

Size, morphology and number of inclusions

Table 3 summarises the data for number, size (given by the average diameter parameter (ADP) calculated as the diameter of a circle with the same area as the inclusion), aspect ratio (calculated as the ratio of maximum dimension to the minimum dimension of each individual particle[5] and area of inclusions for different areas of the bloom before (i.e., cast) and after hot deformation (compression test). Figure 9 shows the size distributions of inclusions in different areas of the bloom before (i.e., cast) and after hot deformation. Figure 10 depicts the number of inclusions per unit area and ADP values for specimens taken from different locations of the bloom for as-cast and deformed conditions. Comparison of the values of the total number and area of inclusions shows that almost in every specimen the main inclusion species present were sulphides. There were noticeable changes in the area of duplex inclusion after hot deformation.

The data for cast and deformed specimens in Table 3 illustrates that the inclusions in the bulk of the bloom (EE and EM) were larger in size, ≈ 4 μm on average, compared with specimens taken from the sub-surface area (AAE and AAM) that were ≈ 1 μm on average.

Comparison of the ADP values for the cast and deformed specimens shows an increase of ADP after hot deformation for each specimen. Table 3 also shows that in the majority of specimens the oxides exhibited the lower aspect ratio, which means that their morphology was more spherical, whereas the duplex inclusions had in most cases the highest aspect ratio among different types of inclusions in each specimen.

This is in agreement with previous observations in which following homogenisation treatment at 1300°C in an AISI 4340 low alloy steel, number of sulphide inclusions decreases after reaching a maximum; however the length of these sulphide inclusions followed an opposite trend[6].

Regarding the numbers and %areas of inclusions in the deformed steel, the total number of inclusions decreased from sub-surface to 30 mm below the surface but not in the bulk. The number of sulphides decreased from sub-surface to 30 mm below the surface and then increased towards the bulk. The number of oxides decreased in the sub-surface area and increased from 30 mm to the bulk. The duplex oxides exhibited exactly the opposite trend compared with the oxides. The %area of sulphides generally decreased between sub-surface and 30 mm below it and then increased towards the bulk, however, in the cast steel the trend in the % area of sulphides was to decrease towards the bulk. The %area of duplex inclusions increased from the sub-surface to 30 mm below it and then decreased to the bulk, but in the cast steel the trend in the % area of duplex inclusions was to decrease towards the bulk. The % area of oxides decreased between sub-surface and 30 mm below it and then increased towards the bulk, but in the cast steel the trend in the % area of oxides was to decrease towards the bulk. It is worth noting that the statistical data for % area in the bulk comes from few large inclusions; whereas in sub-surface, for example, data are collected from significant numbers of smaller inclusions.

Changes in chemistry

The data in Figures 3 to 10 and Table 3 presents a very complicated picture for the changes experienced by the oxide type inclusions between the cast and deformed conditions. Deformation resulted in changes in total numbers and numbers of different types of inclusion, percentages of inclusion types, size and distribution and aspect ratio and %area of inclusion types, and was also accompanied by changes in chemistry and phase transformations in inclusions. There were also small differences between heat-treated and deformed specimens, which would suggest that both temperature and strain energy were responsible for the changes demonstrated by the data in Figures 3 to 7 and 9 to 10 and Table 3.

It is known that in Si rich ferrous melts Mn oxides will be substituted by Mn silicates owing to the high solubility of Mn in liquid silicates[7]. This would explain the high level of Mn silicates in this steel which had ~ 0.25 wt% Si. Decomposition of glassy inclusions and precipitation of crystalline silica is also possible, as reported for the heat treatment of a low carbon steel (0.002-0.01C-0.24Mn-0.035Si) at 1100°C (homologous temperature 0.86) for up to 5hr (Ref. 8) which could be attributed to the extension of the liquid miscibility gap in the $MnO\text{-}SiO_2$ system below the equilibrium solidus temperature into the supercooled liquid[7]. Our data would also suggest crystallisation of glassy inclusions in this steel (Figure 3) and the latter occurred over very short period of time. Figure 11 shows a TTT diagram for the crystallisation of glassy synthetic anorthite[9]. It shows that at about 1150°C crystallisation starts after about 90 s. The rate of crystallisation (time to the nose of the TTT curve) is very sensitive to the composition of inclusions. For example, it has been reported that an increase from 0 to 7% in MgO content in a $CaO\text{-}Al_2O_3\text{-}SiO_2$ mixture resulted in a significant increase in the rate of inclusion crystallisation at 1100 °C (crystallisation started in a shorter period of time)[10].

Change of the chemistry of oxide inclusions in a low carbon steel (0.002-0.01C-0.24Mn-0.035Si) as a result of exposure to elevated temperatures was also observed by Robinson [8] who provided evidence showing devitrified glassy Mn silicate inclusions after heat treatments for 5hr in the range 925 to 1275 °C. His results showed that mainly silica based particles were precipitated after such

treatments. This is in agreement with the results presented in Tables 2a and 2b and Figure 5 where an increase in high silica (SiO_2 content) in sub-surface area is observed as a result of exposure to heat treatment and/or hot deformation. Robinson also reported that glassy silicate inclusions crystallised during soaking time or hot deformation[8, 11].

Two types of Mn silicates, namely manganese orthosilicate ($2MnO.SiO_2$), known as tephroite, and manganese metasilicate ($MnO.SiO_2$), known as rhodonite, have compositions 70.1% MnO and 29.9% SiO_2 and 54.1% MnO and 45.9% SiO2 respectively[7]. These correspond to MnO to SiO_2 ratios respectively 2.34 and 1.18 for tephroite and rhodonite. The data used to construct figures 6 to 7 gives the following values for the MnO to SiO_2 ratio in Mn silicates for the cast steel: 1.74, and 2.5 for the specimens taken from the sub-surface area, 4.19 and 1.35 for the specimens taken 30 mm below the surface, and 7 and 2.53 for the specimens taken from the bulk of the bloom. After hot deformation the MnO to SiO_2 ratio changed as follows: 1.02 and 1.75 for the sub-surface area, 0.51 and 0.53 for 30 mm below the surface, and 0.5 and 0.74 for the bulk. This confirmed that in addition to a noticeable decrease in the percentage of Mn silicate in almost all specimens (Figure 4), the MnO to SiO_2 ratio within the Mn silicate constituents decreased after hot deformation.

The oxide inclusion types present in the steel of this study belong to multi-component oxide systems. Figure 12 shows the ternary systems $CaO\text{-}SiO_2\text{-}Al_2O_3$ and $MnO\text{-}SiO_2\text{-}Al_2O_3$. In these diagrams target regions for chemical composition of so-called deformable inclusions in a high carbon steel killed by Si/Mn are highlighted. It is believed that spessartite ($3MnO.Al_2O_3.3SiO_2$: 36.4%SiO_2, 20.6%Al_2O_3, 43%MnO) has low viscosity, low wettability, good floating properties and good deformability; therefore, it is a preferable type of inclusion that is formed in steel deoxidised by Si/Mn (Ref. 12). Figure 12b shows that Mn silicates, for example tephroite and rhodonite (see above), are also in the desirable region.

In the bloom there were changes in the composition and percentages of inclusions after heat treatment and hot deformation. For example, in specimen AAE the percentages of pseudo- wollastonite and spessartite increased after heat treatment (Figure 5). Comparison of the cast and deformed specimen AAM shows that after hot deformation the percentages of pseudo- wollastonite, spessartite, anorthite and Other increased at the expense of Mn silicate type (Figure 4).

Comparison of Figure 12 with Figures 6 to 7 shows that the inclusions in the bloom were mainly located in low oxidic liquidus temperature regions meaning that the heat treatment and hot deformation occurred at high homologous temperatures T/T_L, in other words under conditions of high diffusivity. Thus, it is suggested that the reported changes in size, number and chemistry of inclusions were influenced by crystallisation reactions and by inclusion coarsening and dissolution phenomena, with the latter driven by increased diffusivity and reduced diffusion distances in the deformed microstructures.

To estimate the diffusion readiness of elements within and around the inclusions, a simple model is used where for the self-diffusivity of austenite γ iron a constant factor F is introduced for each substitutional element:

$$D_{\gamma,i} = F_{\gamma,i} \times A.\exp(\frac{-B}{T})$$

$D_{\gamma,i}$ is in m^2/s and T is in Kelvin[13-14]. Table 4 summarises the values for constant factor (F) and the characteristic diffusion length ($2\sqrt{D * t}$). The data shows that the typical oxygen diffusion length is nearly 25 and 62 microns compared with 7 and 13 for sulphur at the studied temperatures, (1050 and 1150°C, respectively) which would suggest faster kinetics for diffusive adjustment of composition with the matrix or indeed interaction between oxide inclusions, compared with sulphides. The majority of inclusions are in the range of 1-2 micron and diffusion within them should not be too problematic (as witnessed by the devitrification of some oxides into more than one phase, necessarily accompanied by internal diffusion).

Regarding the percentages of inclusions in the deformed steel, in the sub-surface area only the Other inclusion type increased, however, the Other inclusion type did not increase after the heat treatment. The reduced diffusion distances due to hot deformation and the increased diffusivity would be expected to encourage phase transformations, namely precipitation, crystallisation (see above) and coarsening. In the sub-surface areas there were major changes in high silica, Mn silicates due to Mn diffusion from Mn silicates to high silica. Changes in MnO and Al_2O_3 content below the surface exhibited opposite trends between high silica and Mn silicates. The reduction in the percentage of Mn silicates led to an apparent increase in Al_2O_3 + TiO_2 and thus favoured the increase in the percentages of 20% alumina valley and anorthite.

At 30 mm below the surface there were no changes in Other inclusion type and anorthite but the percentages of pseudo-wollastonite and 20% alumina valley increased because of the decrease in the percentage of Mn silicates which affected Al_2O_3 + TiO_2 (thus the link with 20% alumina valley) and the percentages of high silica decreased which affected SiO_2 (thus the link with pseudo-wollastonite). In the bulk there were increases in the percentages of 20% alumina valley and pseudo-wollastonite for the same reasons as for the 30 mm below the surface, due to decreases in the percentages of Mn silicates and high silica.

Changes in the percentages of high silica and Mn silicates were accompanied by opposite changes in the MnO, Al_2O_3 contents in these inclusions. As these changes occurred, the MnO, Al_2O_3 and TiO_2 increased in Other inclusion type, anorthite, 20% alumina valley and pseudo-wollastonite and the MnO and TiO_2 increased in anorthite/galhenite.

CONCLUSIONS

The effect of heat treatment and hot deformation on size, size distribution, distribution and chemistry of non-metallic inclusions in an as-cast high carbon steel was investigated using Gleeble compression simulator at temperature range 1050-1150°C and strains 0.3 and 0.7 at strain rate 1/sec. After hot deformation oxide inclusions which were classified into 11 sub-groups showed changes in chemistry. These changes were different in various locations of the bloom; in sub-surface areas high silica type became dominant phase, at the expense of a reduction in Mn silicates whereas in specimens taken from 30 mm in-depth toward the centre and centre of the bloom an increase in percentages of pseudo-wollastonite and 20% alumina valley was observed. In addition, heat treatment at 1150°C showed that the thermal cycle alone altered the chemical composition of the inclusions; one of the most prominent changes was precipitation of SiO_2 which was also reported in an earlier work by Robinson[8]. Differences in chemistry of oxide species in different locations of bloom, after heat treatment and hot deformation occurred at high homologous temperatures T/T_L, were attributed to reduced diffusion distances due to hot deformation and the increased diffusivity encouraging phase transformations, namely precipitation, crystallisation and coarsening of the inclusions. In addition different micrographs evidencing devitrification of oxide inclusions including different manganese silicates were presented. In terms of sizing of the oxide inclusions, quantitative results showed that the number of oxides per unit area and the average diameter of oxides respectively decreased and increased with increasing distance below the slab surface (or decreasing cooling rate). This suggested that the number and size of inclusions were influenced by solidification condition, crystallisation reactions and by inclusion coarsening and dissolution phenomena, with the latter driven by increased diffusivity and reduced diffusion distances in the deformed microstructures.

ACKNOWLEDGEMENTS

The authors would like to thank the Engineering and Physical Sciences Research Council (EPSRC) for funding this project and Tata Steel UK for supplying the material, the use of automated SEM facilities and their in-house chemistry analysis package. The support and help of Dr Andrew Rose of Tata Steel UK is very much appreciated.

REFERENCES

[1] Pickering F.B., Inclusions, Series: Monograph (Institution of Metallurgists); no.3. London: Institution of Metallurgists, 1979.

[2] M. Faraji, D.P. Wilcox, R. Thackray, A.A. Howe, I. Todd, P. Tsakiropoulos, Quantitative Characterization of Inclusions in Continuously Cast High Carbon Steel, Met. Mat. Trans. B, 2013, submitted.

[3] S. Johansson, "Inclusion Assessment in Steel Using the New Jernkontoret Inclusion Chart II for Quantitative Measurements" in Effect of Steel Manufacturing Processes on the Quality of Bearing Steels edited by J.J.C. Hoo, Baltimore, MD: ASTM, 1988, pp. 250-262.

[4] T.A. Tran, R.P. Thackray, Simulated and Experimental Study of Segregation in Continuously Cast High Carbon Bloom Steel, Iron Steel Technol Conf Proc (AIST – 2012), 2012, vol 1, 1221-1227

[5] J.C. Ross, The Image Processing Handbook, Fourth Edition, CRC Press, 2002, p. 513.

[6] Y.V. MURTY, T.Z. KATTAMIS, R. MEHRABIAN, AND M.C. FLEMINGS, Behavior of Sulfide Inclusions During Thermomechanical Processing of AISI 4340 Steel, METALLURGICAL TRANSACTIONS A, VOLUME 8A, AUGUST 1977, 1275-1282.

[7] C., Benedicks and H. Löfquist, 'Non-metallic inclusions in iron and steel', Chapman & Hall's, 1930.

[8] S.W. Robinson, 'The Plastic Deformation of Non-Metallic Inclusions in Steel', PhD thesis, University of Sheffield, March 1977.

[9] P Rocabois, J.N Pontoire, J Lehmann, H Gaye, Crystallization kinetics of Al2O3–CaO–SiO2 based oxide inclusions, Journal of Non-Crystalline Solids, Volume 282, Issue 1, April 2001, Pages 98–109

[10] P. Rocabois, J.N. Pontoire, H. Gayes, J. Lehmann, C. Gatellier, 'Crystallization of Oxide Inclusions and Their Rheology During Hot Rolling' : Proc. 5th Int. Conf. on Clean Steel, Bulatonfured, Hungarian Mining and Metallurgical Society, Hungary, June 2–4, 1997, pp. 120–129..

[11] F.B. Pickering, S.W. Robinson, The Plastic Deformation and Fracture of Silicate Inclusions in Steel (Chapter 8), Institution of Metallurgists, Inclusions, Monograph (3), 1979, 127-156.

[12] L. Zhang, 'State of the Art in the control of Inclusions in the Cord Steels- a Review', Steel Research Int., 2006, 77, No. 3, 158-169.

[13] A., Howe, 'Simple approaches for solidification and diffusive homogenisation', Ironmaking and Steelmaking, 2011, 38, No. 7, 534-539.

[14] Y-M., Won, B.G., 'Thomas, Simple Model of Microsegregation during Solidification of Steels', 2001, Met. Mat. Trans. A, 32, 7, 1755-1767.

Table 1: Details of the studied specimens and experimental conditions: The prefixes "W" and "H" respectively denotes deformed condition, (e.g. WAAE deformed specimen AAE).

Area in the bloom	**Depth into the bloom**	**Condition**	**Area (mm2)**
AAE	Sub-surface	As-Cast	7.42
AAM	Sub-surface	As-Cast	7.42
DE	30 mm in-depth	As-Cast	3.71
DM	30 mm in-depth	As-Cast	3.71
EE	Centre	As-Cast	3.71
EM	Centre	As-Cast	3.71
WAAE	Sub-surface	1050 ^{o}C, $\varepsilon = 0.7$	7.8
WAAM	Sub-surface	1050 ^{o}C, $\varepsilon = 0.3$	7.8
HAAE	Sub-surface	1150 ^{o}C	2.35
WDE	30 mm in-depth	1150 ^{o}C, $\varepsilon = 0.3$	4.13
WDM	30 mm in-depth	1150 ^{o}C, $\varepsilon = 0.7$	6.16
WEE	Centre	1150 ^{o}C, $\varepsilon = 0.3$	14.50
WEM	Centre	1150 ^{o}C, $\varepsilon = 0.7$	5.89

Table 2a: Changes to different oxide components taken from sub-surface and 30 mm in depth specimens after hot deformation: values are calculated as composition ratio of deformed to cast conditions. Values smaller and greater than one, and ≈ indicate a decrease, an increase, and no change in content of each single oxide component, respectively. It shows apart from High Silica and Mn Silicate, content variation in other types of oxides follows almost a similar trend for both sub-surface and in-depth specimens. MgO and K_2O are not presented here due to their small quantities.

Oxide Types/components	Sub-surface area					30 mm in depth				
	MnO	Al2O3	TiO2	SiO2	CaO	MnO	Al2O3	TiO2	SiO2	CaO
High Silica	0.6	1.6	≈	≈	0.7	3.5	≈	0.8	≈	0.6
Mn Silicate	≈	0.4	≈	1.2	0.1	0.5	9.3	0.5	2.3	2.8
Anorthite	2.3	0.6	11.5	≈	0.2	1.3	0.9	≈	≈	0.5
20% alumina valley	1.6	≈	1.8	1.1	0.5	0.6	≈	0.7	1.3	1.2
pseudo-wollastonite	1.6	0.6	6.7	≈	0.1	1.2	0.9	2.6	≈	0.5
spessartite	0.9	2.6	≈	1.4	--	0.8	1.9	≈	1.3	--

Table 2b: Changes to different oxide components taken from sub-surface area after heat treatment (HAAE): Values smaller and greater than one, and ≈ indicate a decrease, an increase, and no change in content of each single oxide component, respectively. MgO and K_2O are not presented here due to their small quantities.

Oxide Types/components	Sub-surface area				
	MnO	Al2O3	TiO2	SiO2	CaO
High Silica	0.9	0.6	0.2	≈	0.3
Mn Silicate	≈	0.8	≈	≈	≈
Anorthite	≈	1.1	≈	0.9	≈
20% alumina valley	1.5	≈	0.1	≈	0.7
pseudo-wollastonite	≈	0.9	1.5	≈	≈
spessartite	0.7	3.4	≈	1.5	--

Table 3 Data for the number, Average Diameter Parameter, number density, area and aspect ratio of inclusions (sulphide, oxide, and duplex) for different areas of the bloom (C, D, and H represent as-cast, deformed, and heat treated respectively).

Samples		*Average Diameter Parameter (μm)*	*Number of inclusions in 1 mm^2 of the studied area*				*Area of inclusions (μm^2) in 1 mm^2 of the studied area*				*Area (%)*			*Aspect Ratio*			
			Total	*Sulphide*	*oxide*	*Duplex*	*Total*	*Sulphide*	*oxide*	*Duplex*	*Sulphide*	*oxide*	*Duplex*	*all inclusions*	*Oxide*	*Sulphide*	*Duplex*
AAE	C	1.16±0.54	357	325	13	19	456	383	8	65	84	1.8	14.2	1.7±0.7	1.4±0.4	1.7±0.6	2.1±1.4
	H	1.44±0.75	139	105	17	17	288	234	17	37	81.3	5.9	12.8	1.4±1.1	1.4±1.2	1.2±0.3	1.3±0.4
	D	1.79±1.16	263	169	15	79	470	299	7	163	63.7	1.5	34.8	2.1±1.7	1.7±0.6	2.1±1.1	2.3±2.7
AAM	C	1.23±0.52	298	272	11	15	439	384	8	46	87.6	1.9	10.5	1.7±0.6	1.5±0.4	1.7±0.6	2.0±0.8
	D	2.18±1.45	103	61	4	38	553	329	4	219	59.5	0.8	39.7	2.1±1.3	1.5±0.5	2.2±1.4	2.0±1.0
DE	C	3.13±2.65	46	26	1	19	602	222	4	376	36.9	0.7	62.4	2.1±1.2	2.0±0.6	2.1±0.9	2.1±1.6
	D	4.04±2.79	28	10	3	15	516	322	88	106	62.4	17	20.6	1.3±0.6	1.5±0.6	1.2±0.1	1.3±0.7
DM	C	1.83±1.04	144	92	5	47	498	311	3	184	62.5	0.6	36.9	1.9±0.9	1.9±1.0	1.7±0.5	1.9±0.7
	D	3.9±3.52	24	9	3	12	526	385	50	91	73.1	9.5	17.4	1.4±0.7	1.7±1.0	1.3±0.2	1.3±0.3
EE	C	3.79±3.0	17	9	1	7	300	173	5	122	57.7	1.5	40.8	2.5±2.1	1.3±0.2	3.0±2.6	2.0±1.1
	D	4.96±3.65	17	11	4	2	497	398	65	34	80	13.1	6.9	3.7±14.8	4.3±18.3	2.4±1.4	1.9±2.0
EM	C	4.33±2.97	25	9	1	15	512	130	3	378	25.5	0.6	73.9	2.1±1.6	2.2±2.1	1.5±0.3	2.0±1.3
	D	4.58±3.5	27	19	5	3	712	618	78	16	86.8	11	2.2	3.6±3.4	3.6±3.7	3.8±2.9	3.1±2.1

Table 4. Diffusivity data employed in this work; T and t are considered to be 1050 and 1150°C and 30s.

Element	F	A	B	2*Sqrt(D_γ*t) (μm) at T=1050°C	2*Sqrt(D_γ*t) (μm) at T=1150°C
Si	5	0.7×10^{-4}	34400	0.6	1.4
Mn	1.5	0.7×10^{-4}	34400	0.3	0.8
P	20	0.7×10^{-4}	34400	1.1	2.8
Cr	3.5	0.7×10^{-4}	34400	0.5	1.2
Ni	0.7	0.7×10^{-4}	34400	0.2	0.5
Ti	3	0.7×10^{-4}	34400	0.4	1.1
O	10000	0.7×10^{-4}	34400	24.8	61.7
S*	2.4	1	53400	6.6	13.4

* Apart from S which is calculated from the data provided in Won and Thomas 2001 (Re.14) the remaining elements where calculated from the data presented in Howe 2001 (Ref. 13).

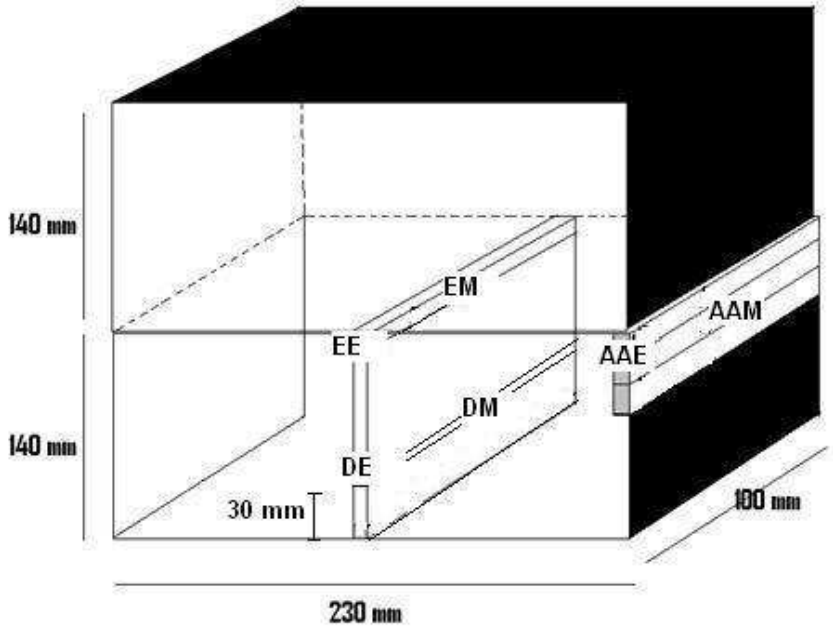

Figure 1: Schematic diagram showing the areas from which samples were selected for characterising inclusions. The facing plane shows the position where the material for this study was cut from the rest of the continuously cast steel. Samples designated AAE and AAM correspond to sub-surface areas, samples DE and DM to areas 30 mm below the surface and samples EE and EM correspond to the bulk (140 mm below the surface).

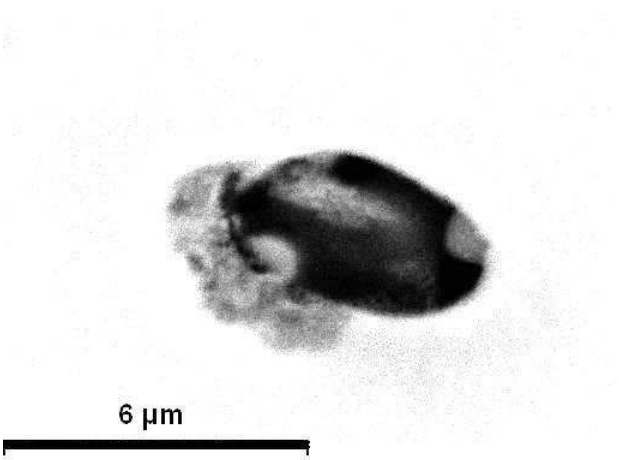

WEE: Mn Silicate

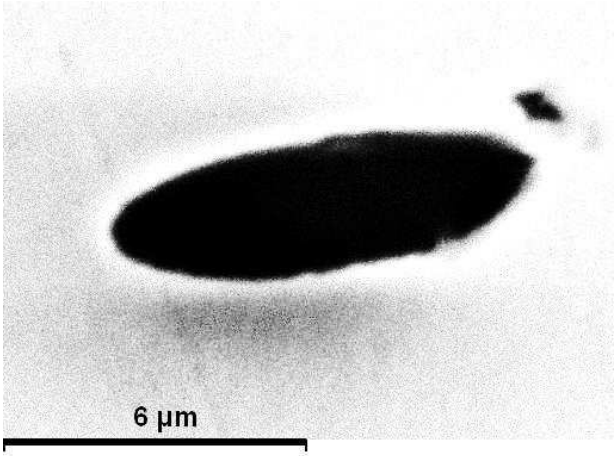

WEE: 20% Alumina Valley

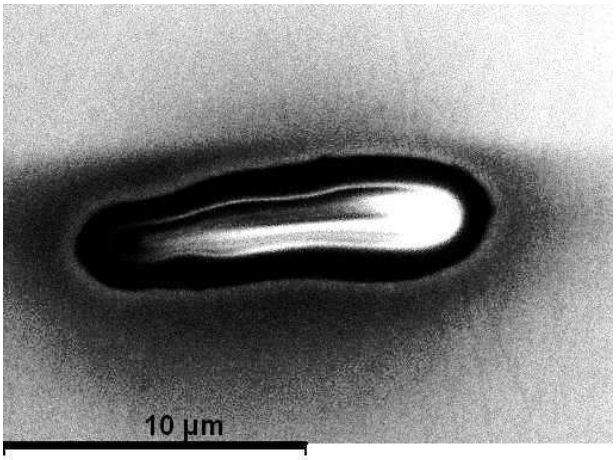

WEE: Pseudo-Wollastonite (CaSiO3):

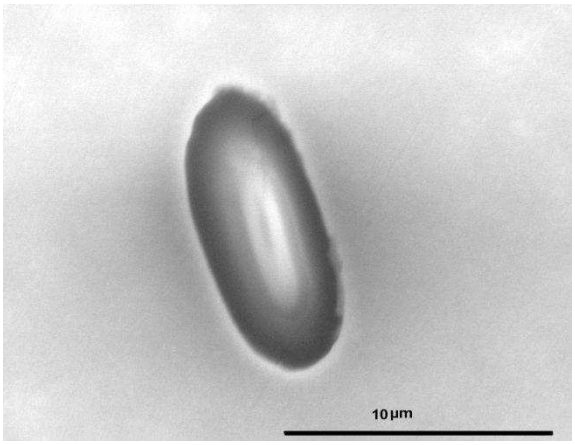

WEE: Anorthite (CaAl2Si2O8)

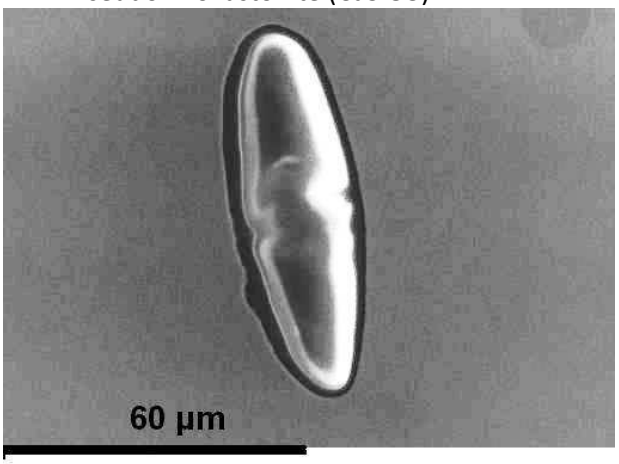

WEE: Anorthite (mainly CaAl2Si2O8)

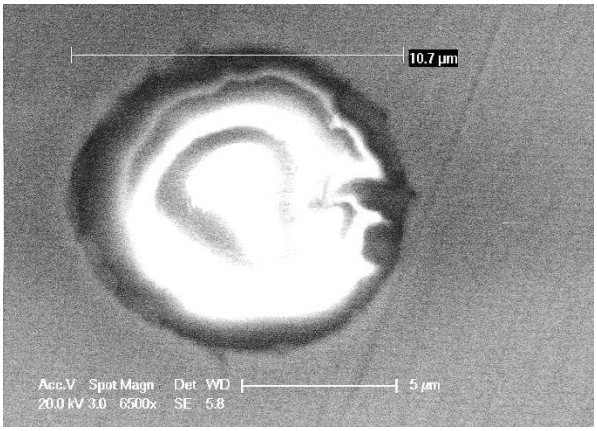

DE: Gehlenite ($Ca_2Al(AlSi)O_7$) (as-cast condition)

Figure 2. Scanning electron micrographs (SE) of complex oxide inclusions in different areas of the bloom.

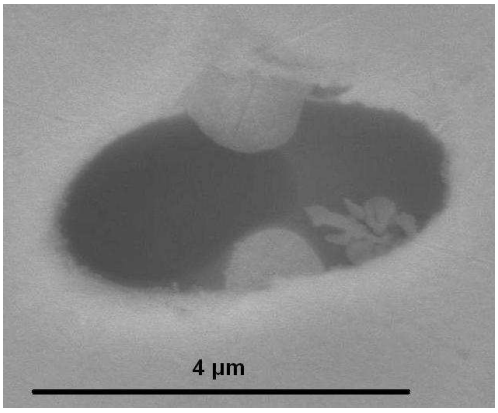

a) Mn Silicate: 65.7%SiO2-24%MnO-5.1%Al2O3-3.7%TiO2-1.5%CaO (WEE)

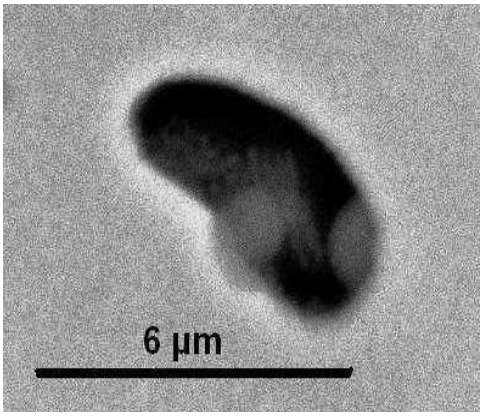

b) Spessartite: 44.5%MnO-37%SiO2-10%TiO2-6%Al2O3-1.6%CaO-1%MgO (WEE)

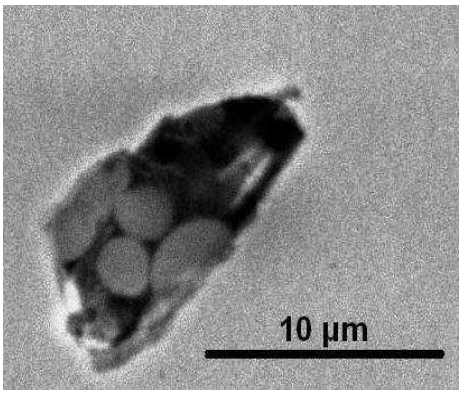

c) Mn Silicate (WEE)

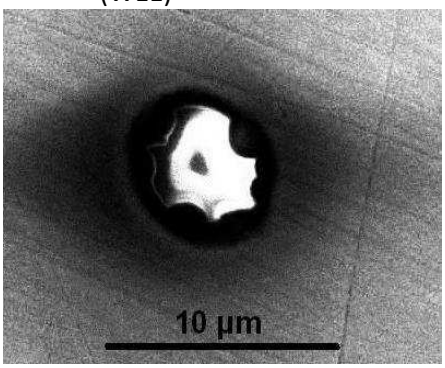

d) 20% Alumina Valley: 51.4%SiO2-13.4%CaO-13.2%Al2O3-12%MnO (WDM)

Figure 3: Scanning electron micrographs (SE) showing evidence of phase transformations in inclusions

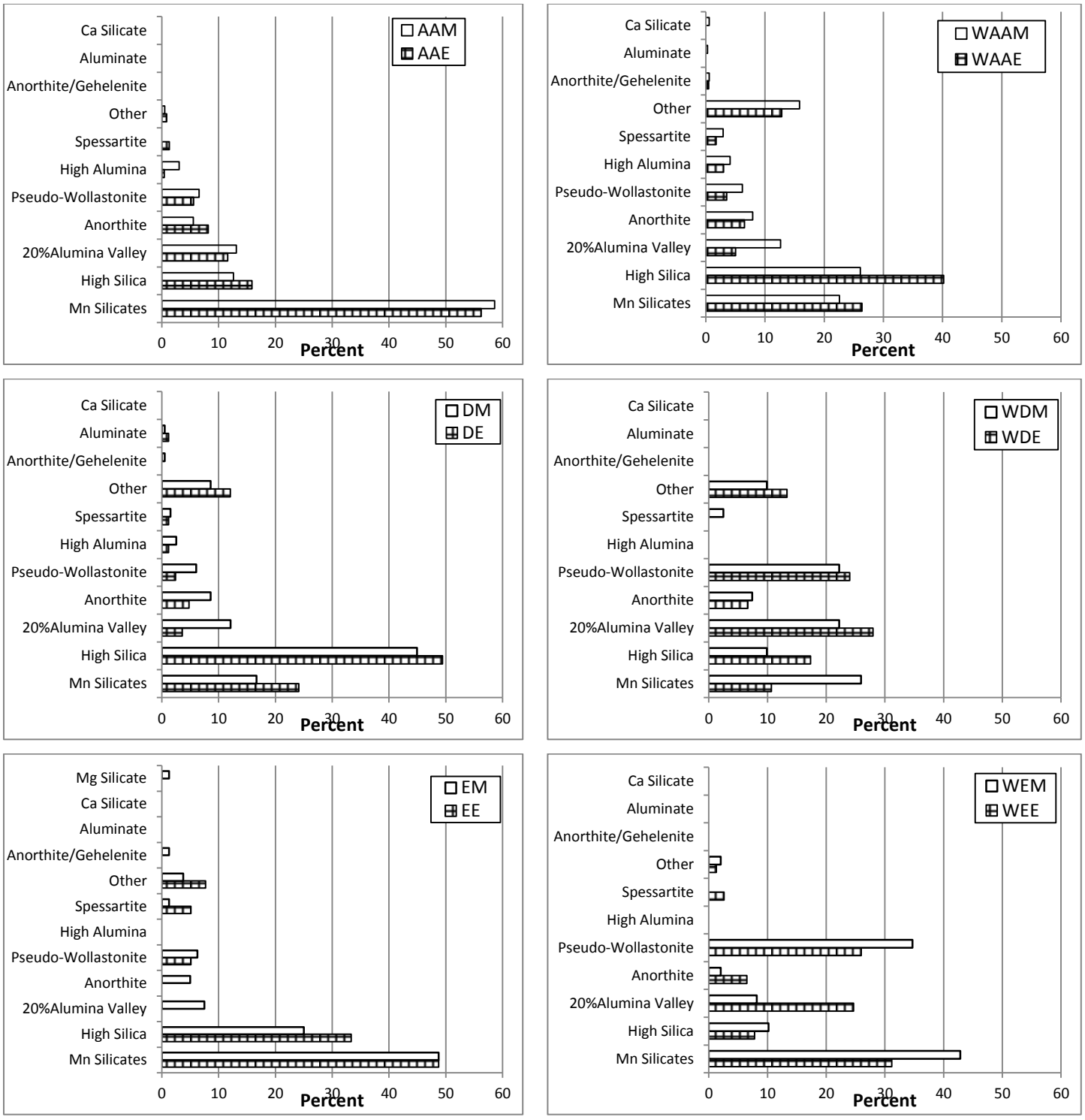

Figure 4: Data for different oxide types (presented as inclusion type versus percentage inclusion) for specimens taken from different areas of the bloom (W: deformed condition). AAE-AAM, DE-DM and EE-EM are taken from sub-surface, 30 mm into the bloom and centre, respectively.

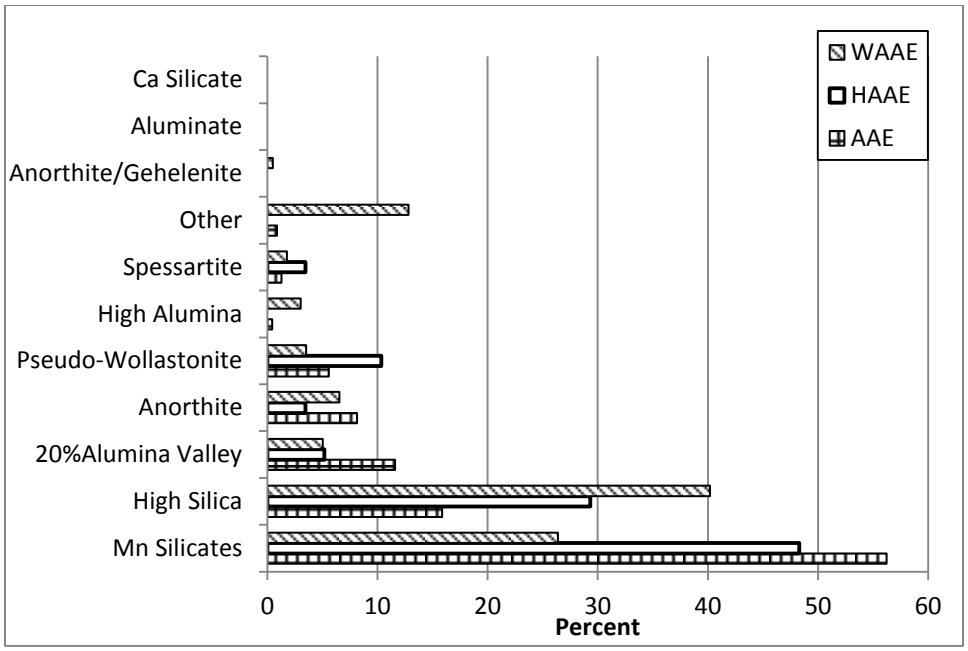

Figure 5: Data for different oxide types (presented as inclusion type versus percentage inclusion) for specimens taken from sub-surface of the bloom (W: deformed condition, H: heat-treated condition).

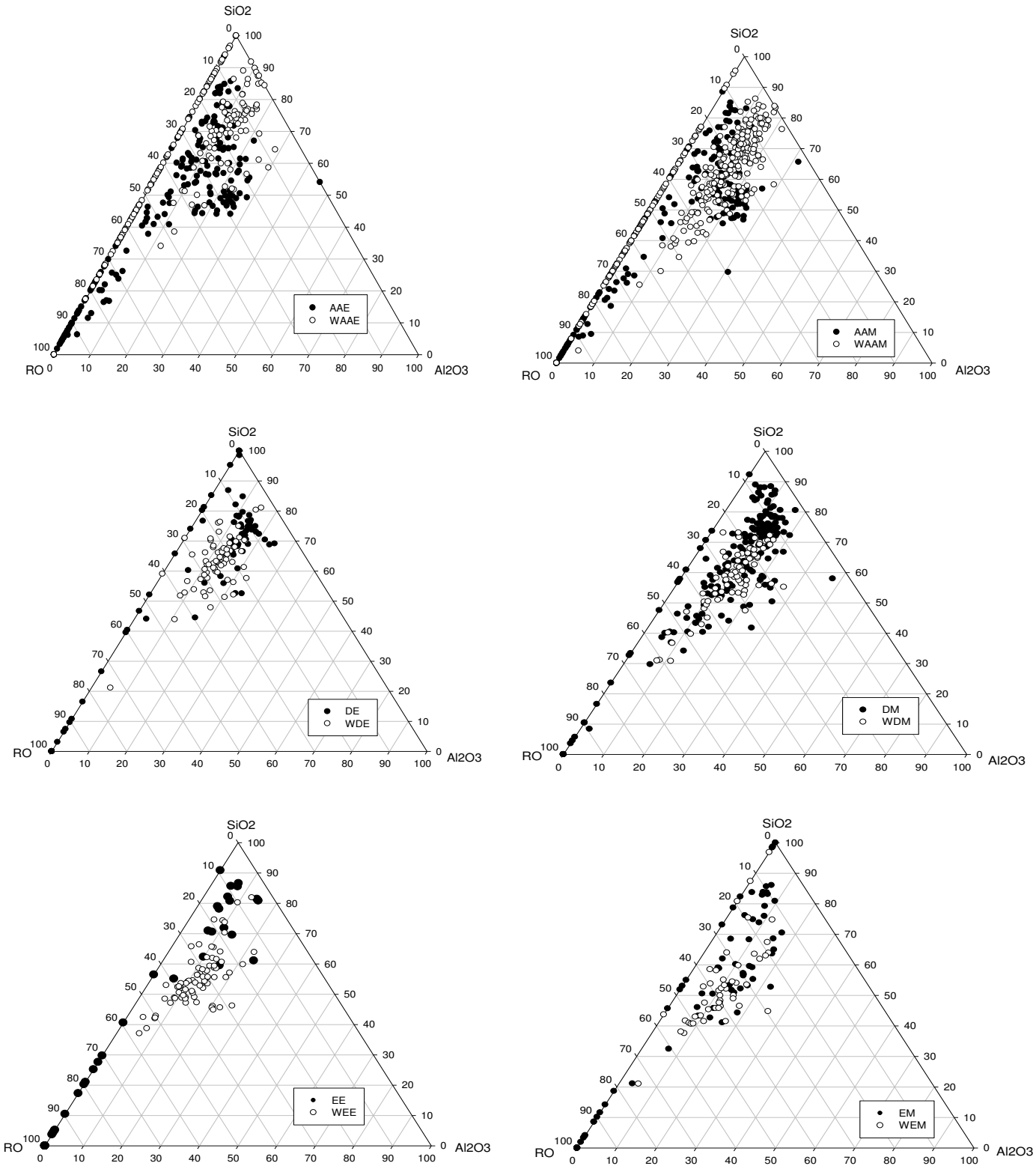

Figure 6: Ternary SiO_2, Al_2O_3, RO (RO = the remaining components mainly MgO-CaO-MnO-TiO_2-K_2O) diagrams showing composition of different oxide inclusions found in different specimens; AAE-AAM, DE-DM and EE-EM are taken from sub-surface, 30 mm into the bloom and centre, respectively.

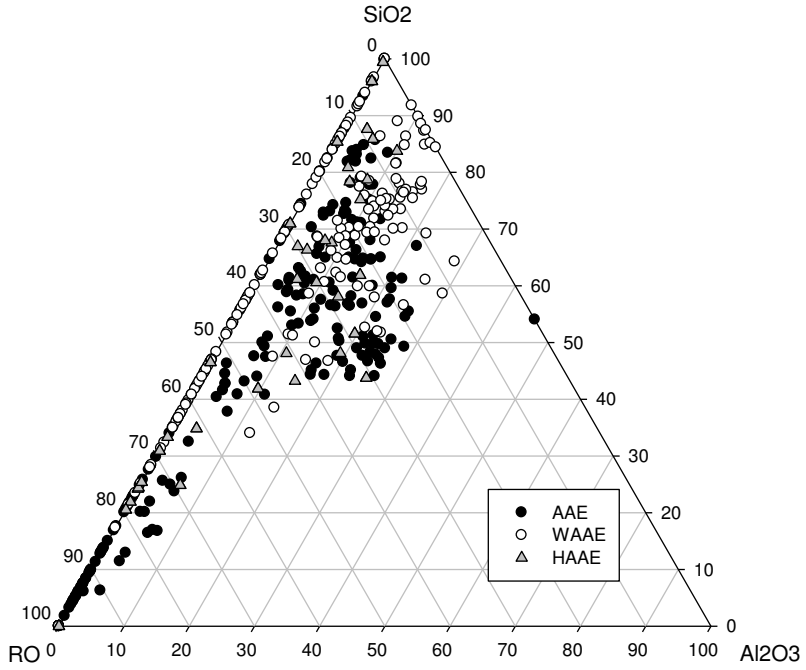

Figure 7: Ternary SiO_2, Al_2O_3, RO (RO = the remaining components mainly MgO-CaO-MnO-TiO_2-K_2O) diagram comparing composition of different oxide inclusions found in subsurface area (AAE) in cast, heat treated and deformed specimen

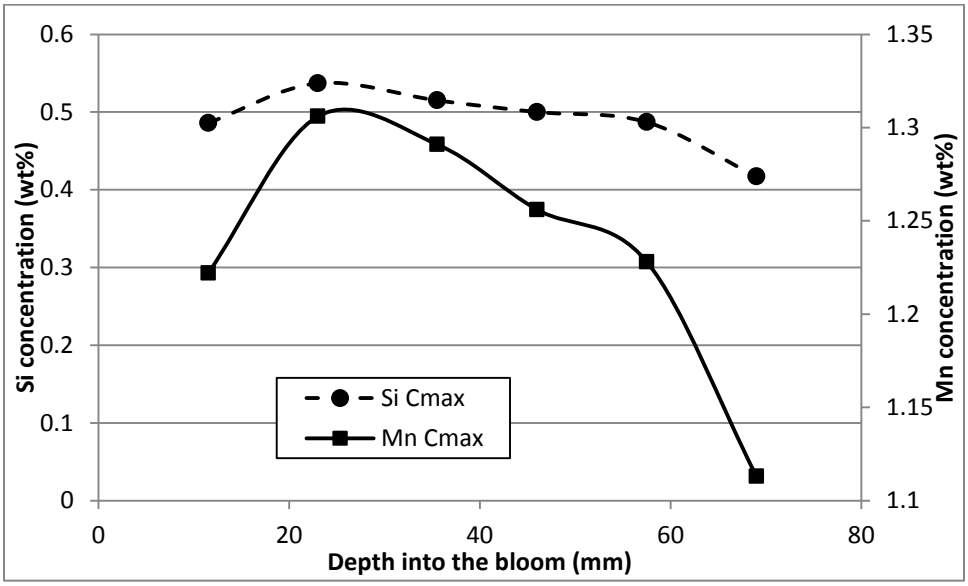

Figure 8: Concentrations of maximum Mn and Si at 1000°C in different locations of the as-cast bloom, showing a micro-segregation with a maximum point of Mn and Si at 30 mm inside the bulk; data adapted from (Ref. 4).

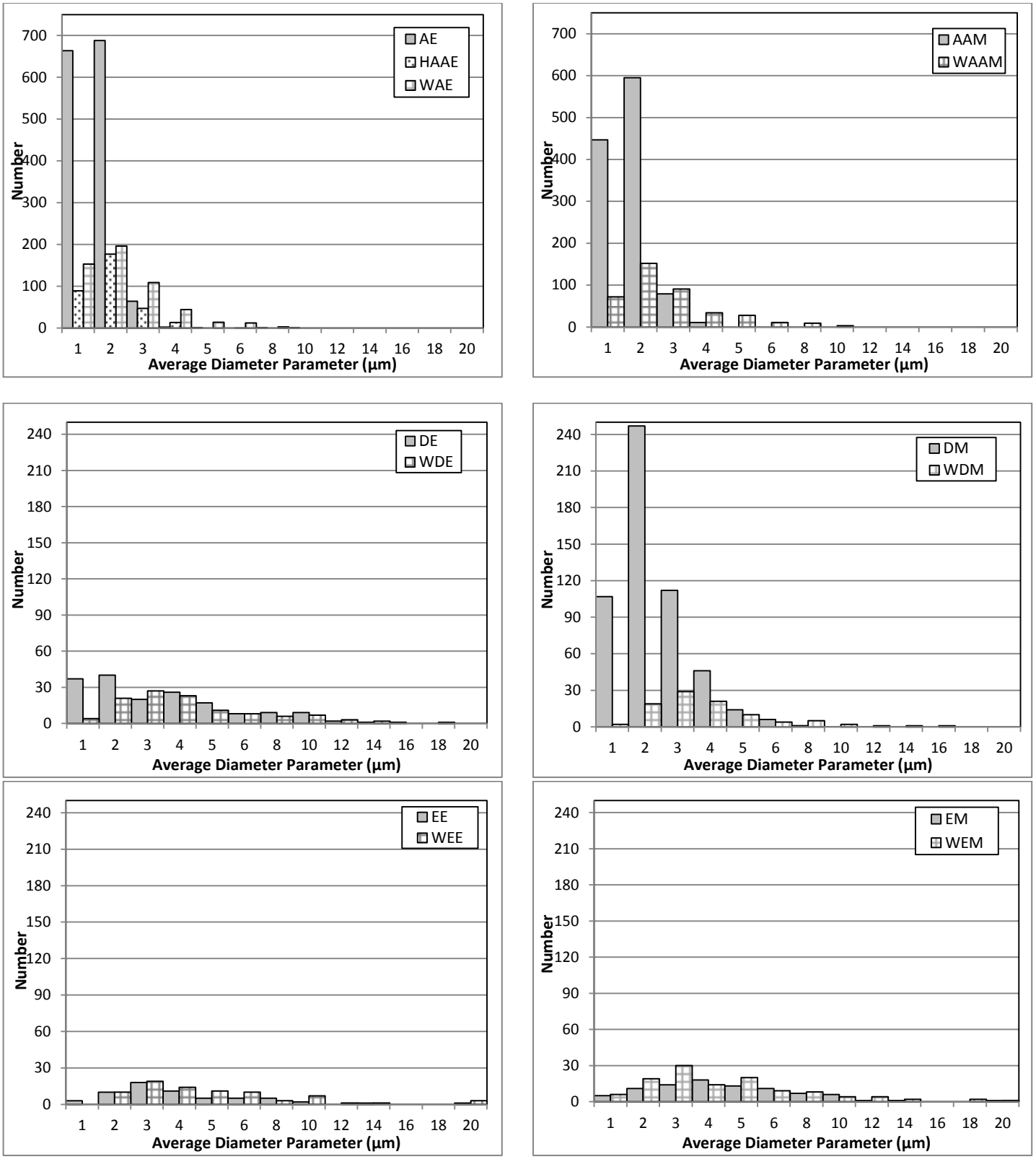

Figure 9: Histograms of size distribution of inclusions in different specimens within examined area of 3.7-3.9 mm^2: AAE and AAM; DE and DM, EE and EM taken from sub-surface, 30 mm into the bloom and centre, respectively ('W' and 'H' denote deformed and heat-treated conditions, respectively).

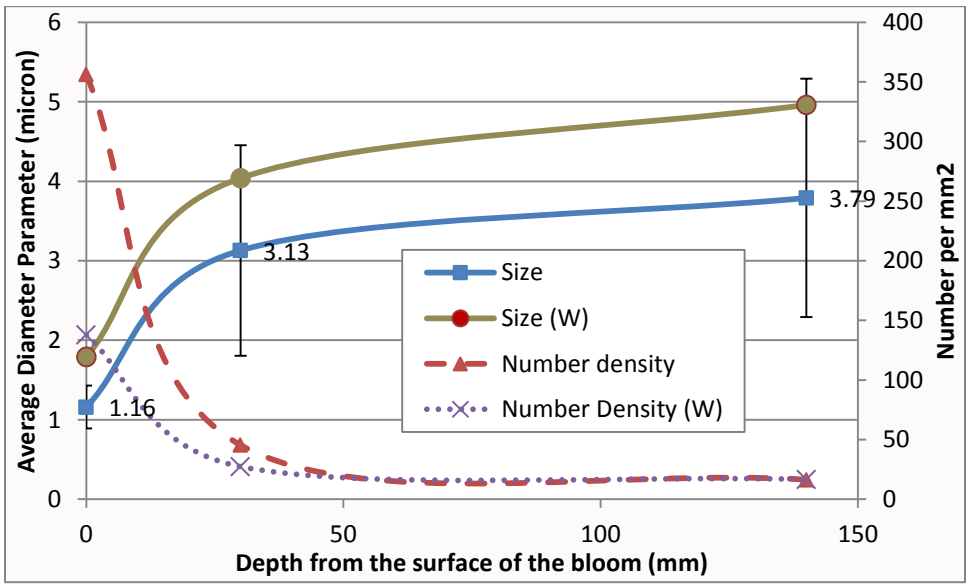

Figure 10: Average Diameter Parameter (Size) and number of inclusions per unit area (number density) for different specimens taken from different locations of the bloom for as-cast and deformed conditions.

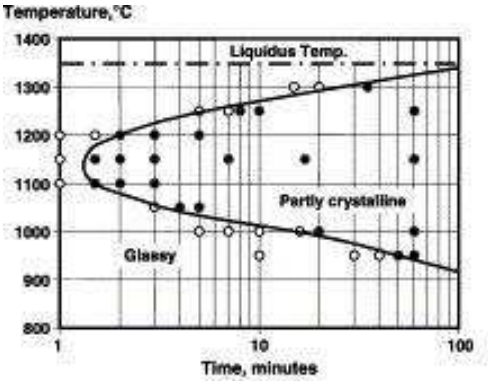

Figure 11. TTT diagram for the 41.3% SiO_2, 33.7% CaO, 24.5% Al_2O_3 composition in anorthite primary phase field. The open and closed circles are glassy and crystallised inclusions, respectively. The line is drawn as a guide for the eye[9].

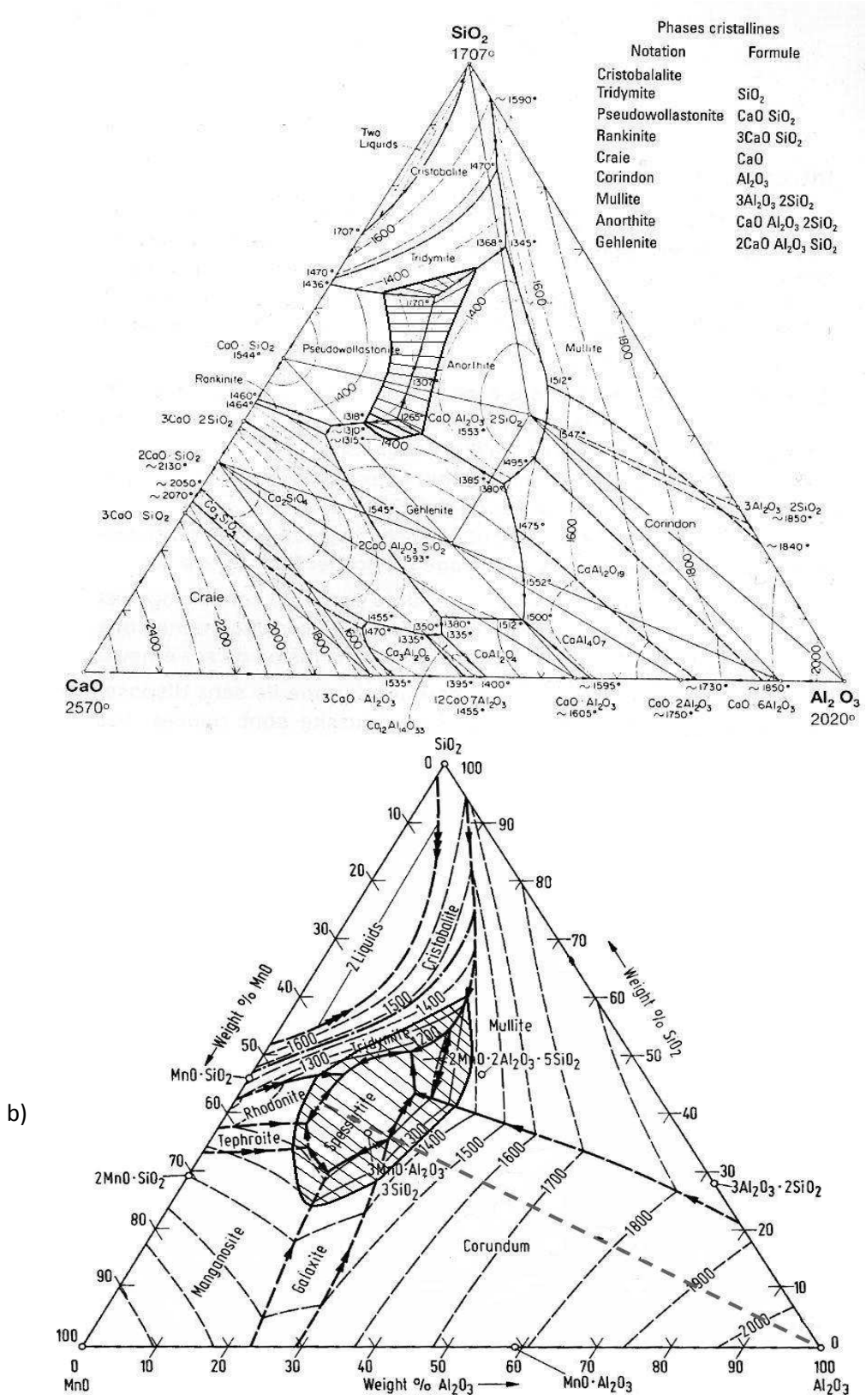

Figure 12. Ternary diagrams for $CaO\text{-}SiO_2\text{-}Al_2O_3$ and $MnO\text{-}SiO_2\text{-}Al_2O_3$ where hatched markings indicate target regions for chemical composition of deformable inclusions in tire cord steel killed by Si/Mn killed steel[12].